Available online at www.sciencedirect.com
SCIENCE DIRECT®
Journal of Sound and Vibration 273 (2004) 755–775
JOURNAL OF SOUND AND VIBRATION
www.elsevier.com/locate/jsvi

Fast maneuver control design for flexible structures using concentrated masses

B.A. Albassam

Department of Mechanical Engineering, King Saud University, P.O. Box 800, Riyadh 11421, Saudi Arabia

Received 10 May 2002; accepted 8 May 2003

Abstract

A method is presented for generating a near-minimum-time control input for flexible structures with the objective of minimizing the maneuver time and the residual energy of the flexible modes. The control design is based on the time-optimal control for the rigid-body mode, which is a bang–bang control with one switching time. The induced vibration due to control spillover to the flexible modes is eliminated through the addition of a concentrated mass placed along the flexible element of the structure. The addition of a concentrated mass at a certain distance along the flexible element of the structure results in a modification of the dynamic characteristics of the structure so that the flexible modes are not excited by the bang–bang control input. Numerical simulations as well as experimental results are provided to demonstrate and validate the effectiveness of the proposed control design method.

1. Introduction

In recent years, there has been a considerable interest in modelling and control of flexible structures. This is due to the use of lightweight materials for the purposes of speed and fuel efficiency. Furthermore, many applications, such as robotic manipulators, disk drive heads and pointing systems in space, are required to maneuver as quickly as possible without significant structural vibrations during and/or after a maneuver.

The time-optimal control for general maneuvers and general flexible structures has posed a challenging problem and is still an open area for research. In particular, the time-optimal control for rest-to-rest slewing maneuvers of flexible structures has been an active area of research, and only limited solutions have been reported in the literature. Solution to the time-optimal control problem of a general flexible system is faced with two main obstacles. First, the number of control

E-mail address: albassam@ksu.edu.sa (B.A. Albassam).

0022-460X/$ - see front matter
doi:10.1016/j.jsv.2003.05.022

switching times is unknown a priori and must be guessed. Second, as the number of modes included in the model is increased, the computer time required by these numerical techniques becomes prohibitive.

In the recent literature, many researchers (see, e.g., Refs. [1–4]) and many others listed in the review paper in Ref. [5] have developed computational techniques that deal with solving time-optimal control of flexible structures. In all of these published works, the exact time-optimal control input, which is of the bang–bang type, is calculated. From an implementation point of view, the bang–bang type of control can easily excite the higher order modes that are neglected in the model.

Other researchers have utilized the simplicity of the time-optimal control design for the rigid-body mode to design a near-minimum-time control for the flexible structure. The main difficulty in applying the minimum-time control input that is based on only the rigid-body mode while neglecting all the flexible modes, is the vibration that takes place during and after the maneuver as a result of control spillover to these modes. This has lead many researchers to modify the bang–bang control input for the rigid-body mode in such a way so as not to excite the flexible modes and, therefore, reduce the vibrations. Junkins et al. [6] and Hecht and Junkins [7] have used an approximation function for the bang–bang control input with the objective of eliminating the instantaneous transition of control magnitudes at a switching time, resulting in a smoother control input. Hurtado and Junkins [8] have used soft constraints in the performance measure that penalize both the weighted combination of elapsed time and the first time-derivative of the control input resulting in a smooth near-minimum-time control input. In a similar approach, Albassam [9] has modified the time-optimal control problem for the rigid-body mode by adding hard constraints on the first and second time-derivative of the control input to eliminate the sudden transition of control magnitudes at a switching time, thereby resulting in a variety of smooth control functions that minimize the energy transfer to the flexible modes. Recently, many researchers [10–12] have added point masses to a beam driven by a harmonic external excitation to either confine or completely eliminate the beam vibrations. These added masses can be thought of as simple reactions that provide transverse forces to the beam.

This paper is concerned with the design of a minimum-time control input for a flexible structure with one rigid-body mode and many flexible modes to perform a quick desired maneuver. The objective is to perform a specified maneuver in minimum time while reducing any residual vibrations at the end of the maneuver. The time-optimal control design is based on only the rigid-body mode. This is motivated by the fact that the solution for the minimum-time control design for the rigid-body mode is easy to calculate and results in the minimum-time solution among the solutions when any of the flexible mode(s) are added to the model.

The basic idea behind the approach of this paper is to change the saturation magnitude for the control input and then select the control input magnitude that gives negligible residual vibrations at the end of the maneuver. Furthermore, if the residual energy for a specified control saturation magnitude is high, then a concentrated mass with a certain magnitude and distance can be mounted along the flexible element in order to change the dynamic characteristics of the structure so that the flexible modes are not excited by the bang–bang control input, resulting in low residual energy.

2. Mathematical modelling

A rigid hub with two flexible appendages as shown in Fig. 1 is considered. A single control actuator at the center of the hub producing a torque $u(t)$ is assumed to be the only input to the system. To derive a mathematical model for this structure, the following are assumed:

1. Flexible appendages deform in an antisymmetric pattern.
2. Euler–Bernoulli beam model is used to represent the flexible appendages.
3. One control torque actuator acting on the center of the rigid hub.
4. Flexible appendage is inextensible, in the sense that the stretch of the neutral axis is negligible.
5. Bending foreshortening is neglected.

Consider a representative flexible appendage with tip and control masses as shown in Fig. 2. The control mass is the added concentrated mass whose magnitude m_c and position x_c are

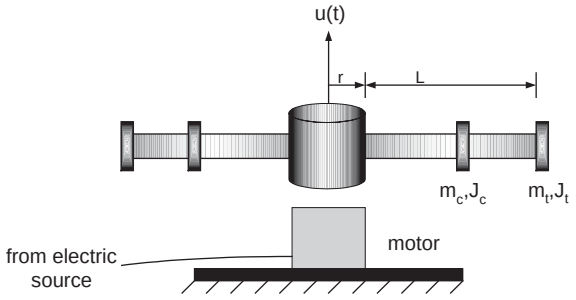

Fig. 1. Schematic for rigid hub with two flexible appendages.

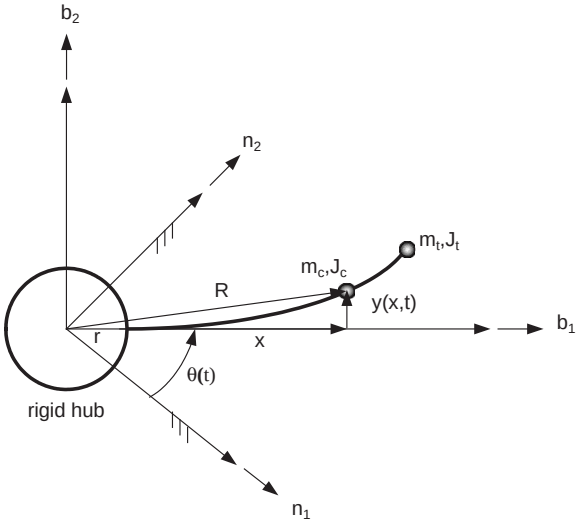

Fig. 2. Deflection in a flexible appendage with rigid-body motion.

determined to yield minimum post-maneuver energy. Two systems of co-ordinates are used to describe the motion of any point on the flexible appendage. These are the right-handed inertial co-ordinates represented by the unit vectors $\mathbf{n}_1$ and $\mathbf{n}_2$, while the unit vectors $\mathbf{b}_1$ and $\mathbf{b}_2$ describe the right-handed body-fixed co-ordinates. The symbol x denotes the co-ordinate of a typical element measured from the outer radius of the hub along the undeformed beam in the direction of the unit vector $\mathbf{b}_1$. The local deformation $y(x,t)$ is measured perpendicular to the $\mathbf{b}_1$-axis.

The inertial position vector $\mathbf{R}$ of a typical deformed point on any of the appendages is

$$\mathbf{R} = (r+x)\mathbf{b}_1 + y\mathbf{b}_2, \tag{1}$$

where r is the radius of the hub. The velocity of this point is given by

$$\dot{\mathbf{R}} = (r+x)\dot{\mathbf{b}}_1 + \dot{y}\mathbf{b}_2 + y\dot{\mathbf{b}}_2, \tag{2}$$

where the over dot indicates differentiation with respect to time. Eq. (2) can be reduced, using basic dynamics, to

$$\dot{\mathbf{R}} = -y\dot{\theta}\mathbf{b}_1 + [(r+x)\dot{\theta} + \dot{y}]\mathbf{b}_2, \tag{3}$$

where θ is the angular displacement of the central hub. The extended Hamilton's principle is used to derive the system equation of motion. In its most general form, Hamilton's principle is given by the following variational statement:

$$\int_{t_1}^{t_2} \delta(T-U)\,\mathrm{d}t + \int_{t_1}^{t_2} \delta W_{nc}\,\mathrm{d}t = 0, \tag{4}$$

where T is the kinetic energy, U is the potential energy, and W_{nc} is the work done by the non-conservative forces and torques.

The system in Fig. 1 is comprised of four elements. These are the central hub, flexible appendages, tip mass and control mass. Therefore, the kinetic energy T is given by

$$T = T_{hub} + T_{appendages} + T_{tip\ mass} + T_{control\ mass}, \tag{5}$$

where the kinetic energy of each element is given by

$$\begin{aligned}
T_{hub} &= \tfrac{1}{2}J_h\dot{\theta}^2,\\
T_{appendage} &= \frac{1}{2}\int_0^L \rho\dot{\mathbf{R}}\cdot\dot{\mathbf{R}}\,\mathrm{d}x,\\
T_{tip\ mass} &= \tfrac{1}{2}m_t\dot{\mathbf{R}}(L)\cdot\dot{\mathbf{R}}(L) + \tfrac{1}{2}J_t(\dot{\theta}+\dot{y}'(L))^2,\\
T_{control\ mass} &= \tfrac{1}{2}m_c\dot{\mathbf{R}}(x_c)\cdot\dot{\mathbf{R}}(x_c) + \tfrac{1}{2}J_c(\dot{\theta}+\dot{y}'(x_c))^2,
\end{aligned} \tag{6}$$

where $(\,)'$ indicates differentiation with respect to x, J_h denotes the rotary inertia for the central hub, ρ represents the appendage mass per unit length, m_t and m_c denote the tip and control mass, respectively, while J_t and J_c denotes the rotary inertia for the tip and control mass, respectively. The dot product of $\dot{\mathbf{R}}\cdot\dot{\mathbf{R}}$ is given by

$$\dot{\mathbf{R}}\cdot\dot{\mathbf{R}} = [(r+x)\dot{\theta}+\dot{y}]^2 + (y\dot{\theta})^2. \tag{7}$$

The system potential energy for the system is given by

$$U = \frac{1}{2}\int_0^L EI(y'')^2 \, \mathrm{d}x, \tag{8}$$

where E is the appendage Modulus of Elasticity and I is the moment of inertia of the appendage cross-sectional area.

The virtual work done by the non-conservative forces and torques for the system in Fig. 1 is given by

$$\delta W_{nc} = u\delta\theta. \tag{9}$$

Upon using the assumed mode method [13], the elastic deformation of the flexible appendage can be described as

$$y(x,t) = \sum_{i=1}^{n} \phi_i(x) q_i(t), \tag{10}$$

where $q_i(t)$ denotes the ith generalized co-ordinate, $\phi_i(x)$ denotes the ith assumed mode shape function which can be determined according to the boundary conditions and n represents the number of flexible mode shapes. Admissible functions [13] for the clamped–free appendage (clamped to the hub) that satisfy the geometrical boundary conditions are used as the assumed mode shapes and are given by

$$\phi_i(x) = 1 - \cos\left(\frac{i\pi x}{L}\right) + \tfrac{1}{2}(-1)^{i+1}\left(\frac{i\pi x}{L}\right)^2. \tag{11}$$

Substituting Eq. (10) into Eqs. (5)–(8) and using the following Lagrange's equations:

$$\begin{aligned} &\frac{\mathrm{d}}{\mathrm{d}t}\left(\frac{\partial T}{\partial \dot{\theta}}\right) - \frac{\partial T}{\partial \theta} + \frac{\partial U}{\partial \theta} = u, \\ &\frac{\mathrm{d}}{\mathrm{d}t}\left(\frac{\partial T}{\partial \dot{q}_i}\right) - \frac{\partial T}{\partial q_i} + \frac{\partial U}{\partial q_i} = 0, \quad i = 1, \ldots, n \end{aligned} \tag{12}$$

the equations of motion can be derived to yield the following matrix form:

$$\begin{bmatrix} m_{\theta\theta} & \mathbf{m}_{\theta q} \\ \mathbf{m}_{q\theta} & \mathbf{m}_{qq} \end{bmatrix} \begin{Bmatrix} \ddot{\theta} \\ \ddot{\mathbf{q}} \end{Bmatrix} + \begin{bmatrix} 0 & \mathbf{0}_{1\times n} \\ \mathbf{0}_{n\times 1} & \mathbf{k}_{qq} \end{bmatrix} \begin{Bmatrix} \theta \\ \mathbf{q} \end{Bmatrix} + \begin{Bmatrix} \mathbf{q}^{\mathrm{T}}\mathbf{N}\mathbf{q}\ddot{\theta} + 2\dot{\mathbf{q}}^{\mathrm{T}}\mathbf{N}\mathbf{q}\dot{\theta} \\ -\mathbf{N}\mathbf{q}\dot{\theta}^2 \end{Bmatrix} = \begin{Bmatrix} u \\ \mathbf{0}_{n\times 1} \end{Bmatrix}, \tag{13}$$

where $(\cdot)^{\mathrm{T}}$ denotes the transpose of $(\cdot)$, and $m_{\theta\theta}$ is a scalar, $\mathbf{m}_{\theta q}$ is $1 \times n$ vector, $\mathbf{m}_{q\theta}$ is $n \times 1$ vector, and $\mathbf{m}_{qq}$, $\mathbf{k}_{qq}$, and $\mathbf{N}$ are $n \times n$ matrices, which are defined as follows:

$$\begin{aligned} m_{\theta\theta} &= \int_0^L \rho(r+x)^2 \, \mathrm{d}x + J_h + m_t(r+L)^2 + J_t + m_c(r+x_c)^2 + J_c, \\ \mathbf{m}_{\theta q}(1,i) &= \int_0^L \rho(r+x)\phi_i \, \mathrm{d}x + m_t(r+L)\phi_i(L) + J_t\phi_i'(L) \\ &\quad + m_c(r+x_c)\phi_i(x_c) + J_c\phi_i'(x_c), \end{aligned}$$

$$\mathbf{m}_{q\theta} = \mathbf{m}_{\theta q}^{\mathrm{T}},$$

$$\mathbf{m}_{qq}(i,j) = \int_0^L \rho\phi_i\phi_j \,\mathrm{d}x + m_t\phi_i(L)\phi_j(L) + J_t\phi_i'(L)\phi_j'(L) + m_c\phi_i(x_c)\phi_j(x_c) + J_c\phi_i'(x_c)\phi_j'(x_c),$$

$$\mathbf{k}_{qq}(i,j) = \int_0^L EI\phi_i''\phi_j'' \,\mathrm{d}x,$$

$$\mathbf{N}(i,j) = \int_0^L \rho\phi_i\phi_j \,\mathrm{d}x + m_t\phi_i(L)\phi_j(L) + m_c\phi_i(x_c)\phi_j(x_c). \tag{14}$$

The above non-linear dynamic equations of motion provide a relatively accurate mathematical description of the system motion and can be used for simulation purposes. However, due to the non-linearity, this model usually imposes severe constraints on the design of controllers [14]. Therefore, it is desirable to develop a linear and finite dimensional model for controller design and implementation purposes. Under the assumption of small appendage deflection ($y(L,t)/L<0.1$), the linearized model is obtained by setting all the non-linear terms in Eqs. (13) to zero [15,16] and can be expressed as

$$\mathbf{M}\ddot{\mathbf{z}} + \mathbf{K}\mathbf{z} = \mathbf{D}u, \tag{15}$$

where $\mathbf{z} = [\theta\ q_1\ q_2\ \ldots\ q_n]^{\mathrm{T}}$ and $\mathbf{D} = [1\ 0\ 0 \ldots 0]^{\mathrm{T}}$ are $(n+1)\times 1$ vectors and $\mathbf{M}$ and $\mathbf{K}$ are $(n+1)\times(n+1)$ mass and stiffness matrices, respectively, and defined as

$$\mathbf{M} = \begin{bmatrix} m_{\theta\theta} & \mathbf{m}_{\theta q} \\ \mathbf{m}_{q\theta} & \mathbf{m}_{qq} \end{bmatrix} \quad \text{and} \quad \mathbf{K} = \begin{bmatrix} 0 & \mathbf{0} \\ \mathbf{0} & \mathbf{k}_{qq} \end{bmatrix}. \tag{16}$$

3. Bang–bang control input

In this section, a control input $u(t)$ is designed for the system in Eq. (15) to perform a rest-to-rest maneuver from the initial condition $\mathbf{z}(0) = [0\ 0 \ldots 0]^{\mathrm{T}}$ to the final condition $\mathbf{z}(t_f) = [\theta_f\ 0\ 0 \ldots 0]^{\mathrm{T}}$ and in minimum time. From optimal control theory, it is known that the control input structure is of the bang–bang type, which can be characterized by its switching times. Many researchers (see, e.g., Ref. [1]) have utilized this characteristic to develop numerical techniques that transfer the time-optimal control problem into parameter optimization problem in terms of the control switching times. They have also noted that as the number of flexible modes in the model increases, the number of control switching times also increases, thereby, making the optimal control problem more difficult, or impossible, to solve, especially, when the number of modes becomes quite large. On the contrary, the problem becomes very simple when only the rigid-body mode is considered in the model. In this case, the control input is shown in Fig. 3, which is a bang–bang control input that can be characterized by only one switching time t_{s1} and a final time t_f. The control input $u(t)$, shown in Fig. 3, is constrained according to

$$-u_{max} \leqslant u(t) \leqslant u_{max}. \tag{17}$$

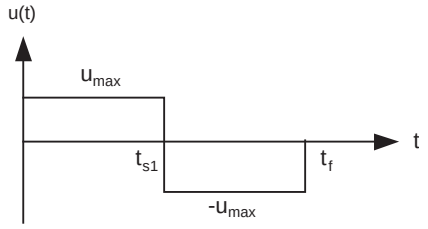

Fig. 3. Bang–bang control input for the rigid-body mode.

The system in Eq. (15) can be transformed into the decoupled modal equations using the eigenvectors of the system to the form

$$\ddot{\beta} = a_0 u, \tag{18}$$

$$\ddot{\eta}_i + \omega_i^2 \eta_i = a_i u, \quad i = 1, \ldots, n, \tag{19}$$

where $\beta(t)$ is the rigid-body co-ordinate, $\eta_i(t)$ is the ith modal co-ordinate, and ω_i is the ith frequency. The scalars $a_i,\ i = 0, \ldots, n$ are defined by

$$[a_0 \ \ a_1 \ \ \ldots \ \ a_n]^{\mathrm{T}} = \mathbf{\Phi}^{\mathrm{T}}\mathbf{D}, \tag{20}$$

where $\mathbf{\Phi}$ is the matrix of eigenvectors.

The initial and final conditions, $\mathbf{z}(0)$ and $\mathbf{z}(t_f)$, can also be transformed to the modal co-ordinates as

$$[\beta(0) \ \ \eta_1(0) \ \ \ldots \ \ \eta_n(0)]^{\mathrm{T}} = \mathbf{\Phi}^{\mathrm{T}}\mathbf{M}\mathbf{z}(0), \tag{21}$$

$$[\beta(t_f) \ \ \eta_1(t_f) \ \ \ldots \ \ \eta_n(t_f)]^{\mathrm{T}} = \mathbf{\Phi}^{\mathrm{T}}\mathbf{M}\mathbf{z}(t_f). \tag{22}$$

Analytical solutions for the control switching and final times do exist in the literature (see, e.g., Ref. [17]) and are given by

$$t_{s1} = \sqrt{\frac{\beta(t_f)}{u_{max}a_0}}, \tag{23}$$

$$t_f = 2t_{s1}. \tag{24}$$

4. Numerical examples

4.1. Example 1

As an example to illustrate the numerical procedure and show its effectiveness, the time-optimal single-axis maneuver problem for a system consisting of a rigid hub with two uniform elastic appendages attached to it as shown in Fig. 1 is considered. A single actuator that exerts an external torque on the rigid hub controls the motion of the system. It is desired to rotate the flexible structure by a certain angular displacement as quickly as possible while suppressing the

vibration at the end of the maneuver to achieve good pointing accuracy. The above design method is applied to a relatively small and large size flexible structures. The first one has the material properties, dimensions and maneuver specifications listed in Table 1. The data are taken from Ref. [13, p. 190] with slight modifications. Ten flexible modes are retained in the evaluation model making the size of the mass and stiffness matrices, in Eq. (15), 11×11.

If the bang–bang control input for the rigid-body mode is applied to the structure in Table 1 while changing the maximum control magnitude and without the addition of control mass, the variation of the residual energy versus the maximum control magnitude u_{max} is shown in Fig. 4. As seen from this figure, if the maximum control magnitude u_{max} is approximately 3 N m or in the range between 12 and 13 N m, then the bang–bang control input for the rigid-body mode can be applied without considering the flexible modes and should not expect any vibrations at the end of the maneuver. On the contrary, if the maximum control magnitude u_{max} is equal to 6 or 20 N m, then the rigid hub would oscillate at the end of the maneuver leading to imprecise maneuvering. The rigid hub attitude simulations for two different maximum control magnitudes, $u_{max} = 11.65$ and 20 N m, are shown in Fig. 5. The corresponding maneuver times, t_f, are 3.1993 and 2.4418 s, respectively. Using Fourier analysis, the first three frequencies in the two bang–bang control input signals are calculated and shown in Table 2 along with the first three flexible modes natural frequencies of the system. Clearly, the bang–bang control input with control saturation magnitude $u_{max} = 11.65$ N m has frequencies that are farther away from the natural frequencies of the system compared with the case when the control saturation magnitude $u_{max} = 20$ N m.

If the actuator available can only supply a maximum control magnitude u_{max} equal to 20 N m, then a concentrated mass (or point mass) may be added with a magnitude m_c and position x_c along the appendage in order to modify the dynamic characteristics of the structure so that the bang–bang control input for the rigid-body mode does not excite the flexible modes, thus, resulting in almost zero residual energy. A Matlab® program is written to calculate the residual energies for a given range of control mass magnitudes m_c and position x_c. An output of this program is shown in Fig. 6 for $m_c = 0 \ldots 5$ kg, $x_c = 0 \ldots 2$ m and $u_{max} = 20$ N m. As seen from this figure, many combinations of mass magnitudes and positions can be chosen that result in negligible residual energies. It is obvious that our selection should be based on the combinations

Table 1
System dimensions, appendage material, and maneuver specifications

Radius of the rigid central hub, r	0.3048 m
Length of one appendage, L	2 m
Appendage material Young's modulus, E	7.5842×10^{10} N/m^2
Appendage width	3.175×10^{-3} m
Appendage height	0.1524 m
Cross-section moment of area, I	4.0648×10^{-10} m^4
Appendage material density, ρ	1.3017 kg/m
Command slew angle, θ_f	40.00°
Hub rotary inertia	10.8465 kg m^2
Tip mass, m_t	2 kg
Tip rotary inertia, J_t	0.0024 kg m^2

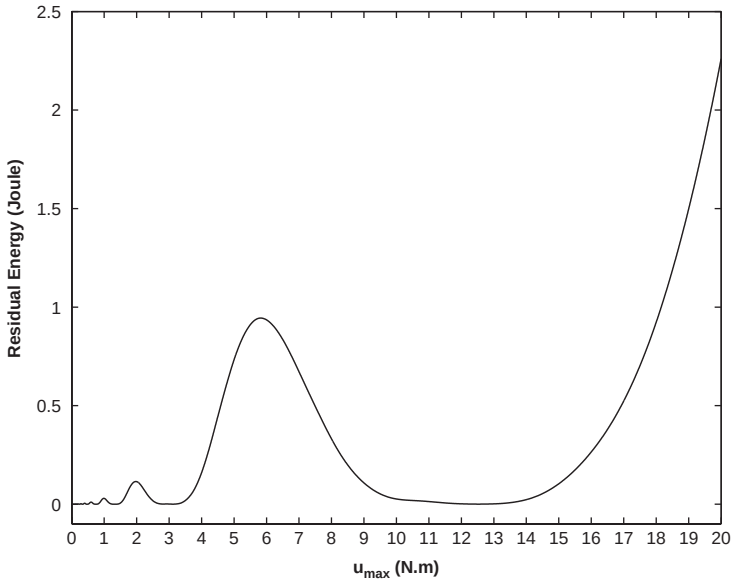

Fig. 4. Residual energies corresponding to maximum control magnitude variations.

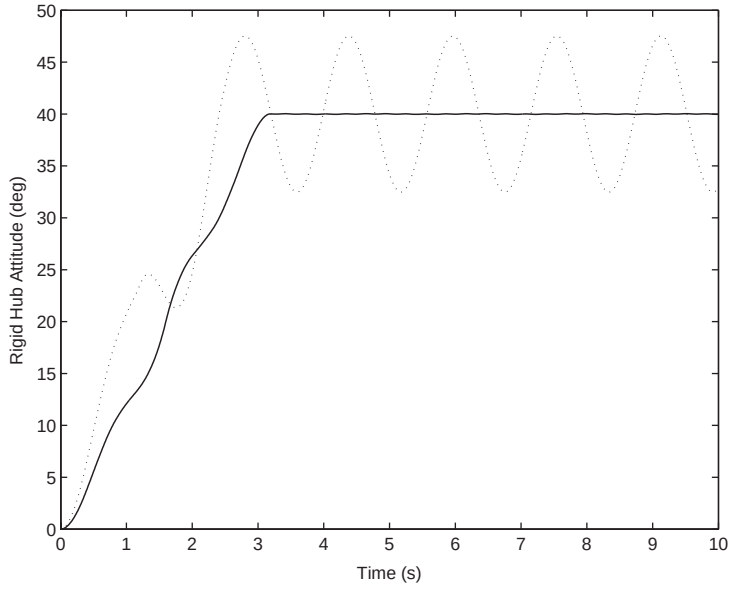

Fig. 5. Rigid hub attitude simulations for maximum control magnitudes $u_{max} = 11.65$ N m (solid line, $t_f = 3.1993$ s, residual energy = 0.0045 J) and $u_{max} = 20$ N m (dotted line, $t_f = 2.4418$ s, residual energy = 2.2604 J).

of mass magnitude and position resulting in the lowest possible maneuver time. Therefore, a control mass magnitude $m_c = 4.2$ kg and position $x_c = 1.6$ m can be chosen and the corresponding rigid hub attitude simulation with and without the control mass is shown in

Table 2
First three natural frequencies, in Hz, for the system and frequencies in the control signals for $u_{max} = 11.65$ and 20 N m

System natural frequencies	0.633	3.287	9.860
$u_{max} = 11.65$ N m	0.313	0.938	1.563
$u_{max} = 20$ N m	0.410	1.229	2.048

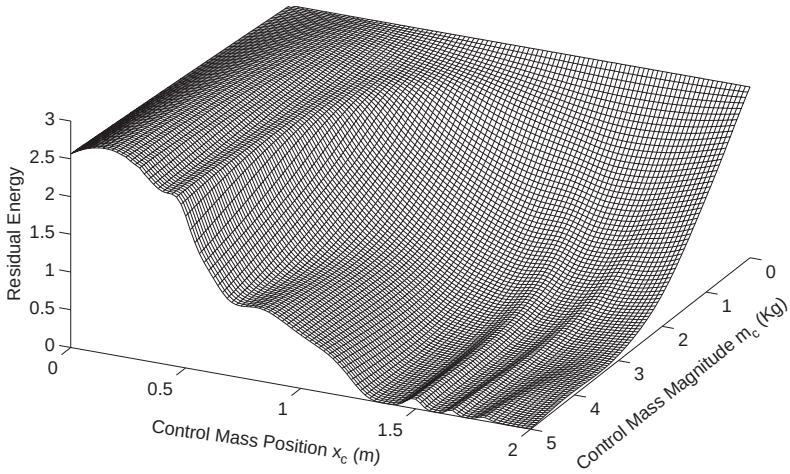

Fig. 6. Residual energies corresponding to control mass and distance variations.

Fig. 7. In this case, the maneuver time is equal to 3.1965 s. The added control mass amounts to only 3.5% of the total mass of the structure. The rigid hub attitude simulation in Fig. 7 shows a significant post-maneuver energy reduction when the control mass is added to the system at the expense of 31% increase in maneuver time. Using Fourier analysis, the first three frequencies in the two bang–bang control inputs, with and without the addition of a control mass, are calculated and are shown in Table 3, along with the first three flexible modes natural frequencies of the system. Clearly, the addition of a control mass lowered the frequencies in the control input signal compared with the case of no control mass addition and, therefore, widened the gap between the control input signal frequencies and the natural frequencies of the system, resulting in a reduced level of flexible modes excitation. The strength of this control design method can also be evidenced from Fig. 8, which shows the time simulation of the tip position defined by [18]

$$\mathrm{TP} = L\theta(t) + y(L, t), \tag{25}$$

where TP stands for tip position in (m).

If the designed bang–bang control input for the rigid-body mode with the control mass is applied to the non-linear system model, Eq. (13), then the effect of addition of the control mass ($m_c = 4.2$ kg, $x_c = 1.6$ m) on the rigid hub attitude is shown in Fig. 9. The addition of the control mass has reduced the post-maneuver energy for the non-linear system by 93% at the expense of 31% increase in maneuver time. Furthermore, the tip mass position for the non-linear system

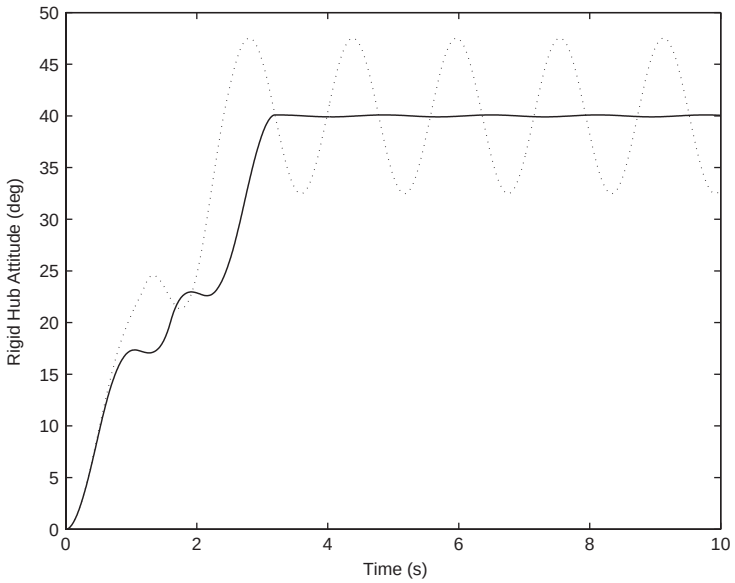

Fig. 7. Rigid hub attitude simulations without control mass (dotted, $t_f = 2.4418$ s, residual energy = 2.2604 J) and with control mass (solid, $m_c = 4.2$ kg, $x_c = 1.6$ m, $t_f = 3.1965$ s, residual energy = 0.0007 J) for the linear model.

Table 3
First three natural frequencies, in Hz, for the system and frequencies in the control signal for $u_{max} = 20$ N m with and without control mass

System natural frequencies (Hz)	0.633	3.287	9.860
$u_{max} = 20$ N m (without control mass)	0.410	1.229	2.048
$u_{max} = 20$ N m (with control mass)	0.313	0.939	1.564

model, when the bang–bang control input for the rigid-body mode is applied, is shown in Fig. 10 both with and without adding the control mass. As a result of the addition of the control mass, the tip mass position residual vibration amplitude has been reduced by 88%. The slight disagreement between the linear and non-linear system model behaviors is attributed to the large tip mass deflection that is larger than $0.1L$, which is the maximum tip mass deflection allowed to neglect the non-linear terms in Eq. (13).

4.2. Example 2

In this example, a rigid hub with two flexible appendages having a size that is relatively larger than that considered in Example 1 is considered. Table 4 lists the material properties, dimensions, and maneuver specifications for the system. It is desired to select the control mass magnitude m_c and position x_c to perform a rapid 45° maneuver with negligible residual energy. The residual energy variation as the control mass magnitude and position take the values $m_c = 0 \ldots 10$ kg and $x_c = 0 \ldots 20$ m, respectively, is shown in Fig. 11. As seen from this figure, many combinations of control mass magnitudes and positions can be selected to yield negligible residual energies.

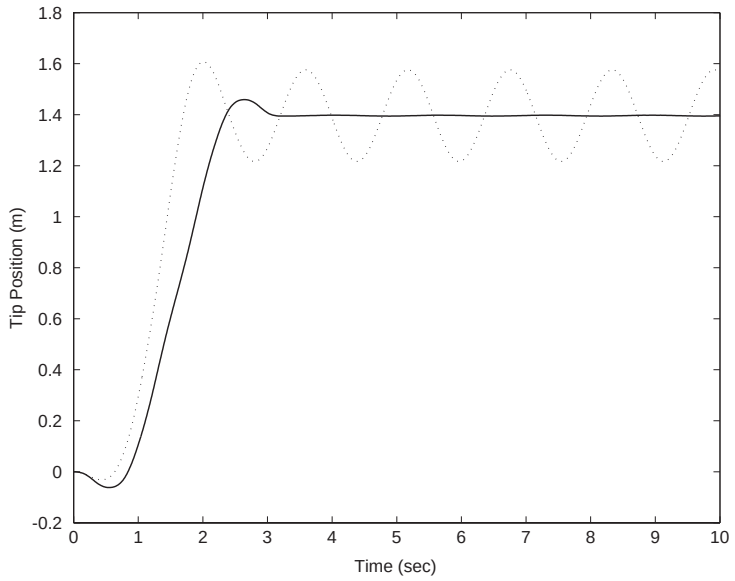

Fig. 8. Tip mass position simulations without control mass (dotted) and with control mass (solid, $m_c = 4.2$ kg and $x_c = 1.6$ m) for the linear model.

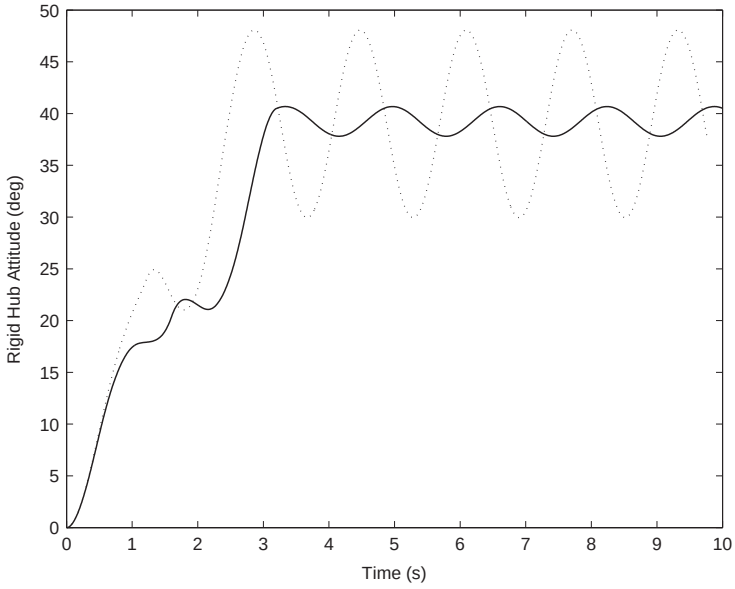

Fig. 9. Rigid hub attitude simulations without control mass (dotted, $t_f = 2.4418$ s, residual energy = 3.3505 J) and with control mass (solid, $m_c = 4.2$ kg, $x_c = 1.6$ m, $t_f = 3.1965$ s, residual energy = 0.0676 J) for the non-linear model.

Selecting the combination with the lowest possible value of control mass magnitude and position, $m_c = 1.7$ kg and $x_c = 11.2$ m, results in the rigid hub attitude simulation shown in Fig. 12. The corresponding maneuver times are equal to 3.7719 and 5.4887 s both without and with control

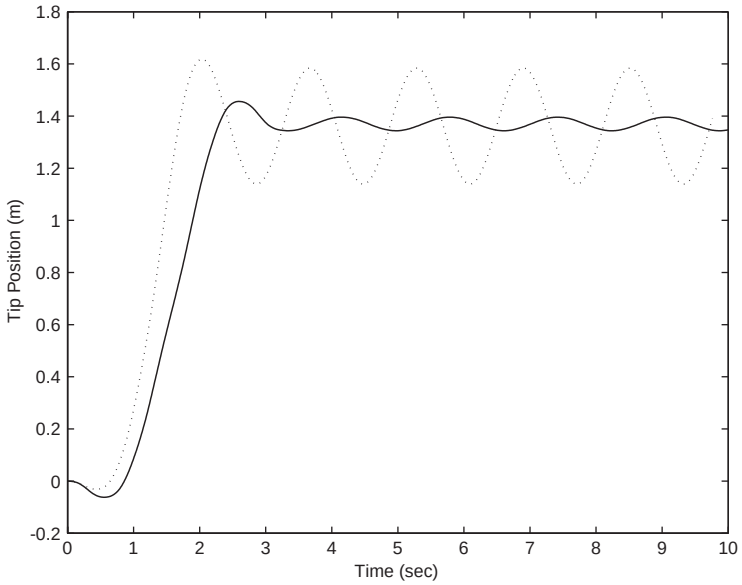

Fig. 10. Tip mass position simulations without control mass (dotted) and with control mass (solid, $m_c = 4.2$ kg and $x_c = 1.6$ m) for the non-linear model.

Table 4
System dimensions, appendage material, and maneuver specifications

Radius of the rigid central hub, r	1.00 m
Length of one appendage, L	20.00 m
Appendage material stiffness, EI	1500.00 N m^2
Appendage material density, ρ	0.04096 kg/m
Mass of the rigid central hub	400.00 kg
Command slew angle, θ_f	45.00°
Total rotational inertia, J^*	2081.97547 kg m^2
Maximum torque available, u_{max}	100 N m

mass, respectively. The added mass magnitude amounts to only 0.85% of the total mass of the structure. The addition of the control mass has almost eliminated the post-maneuver energy at the expense of 45% increase in maneuver time. The tip mass positions both with and without the addition of the control mass are shown in Fig. 13.

If the designed bang–bang control input for the rigid-body mode with the control mass is applied to the non-linear system model, Eq. (13), then the effect of addition of the control mass ($m_c = 1.7$ kg, $x_c = 11.2$ m) on the rigid hub attitude is shown in Fig. 14. The addition of the control mass has reduced the post-maneuver energy for the non-linear system by 99% at the expense of 45% increase in maneuver time. Furthermore, the tip mass position resulting from the non-linear model is shown in Fig. 15 for both with and without the control mass. As a result of the addition of the control mass, the tip mass position residual vibration

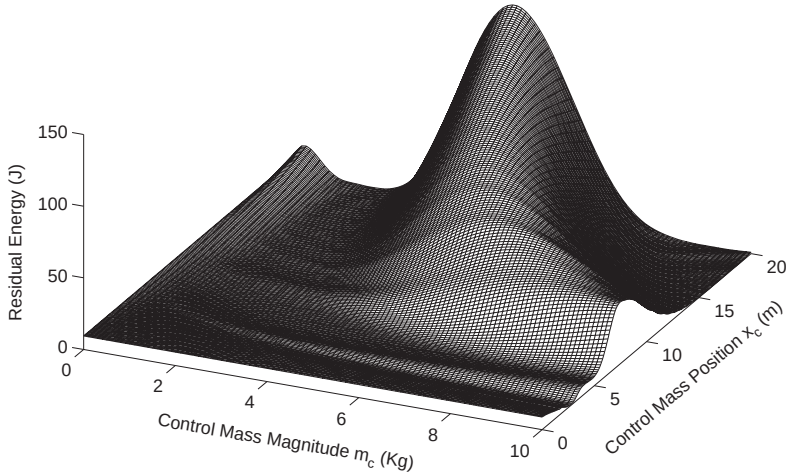

Fig. 11. Residual energies corresponding to control mass and distance variations.

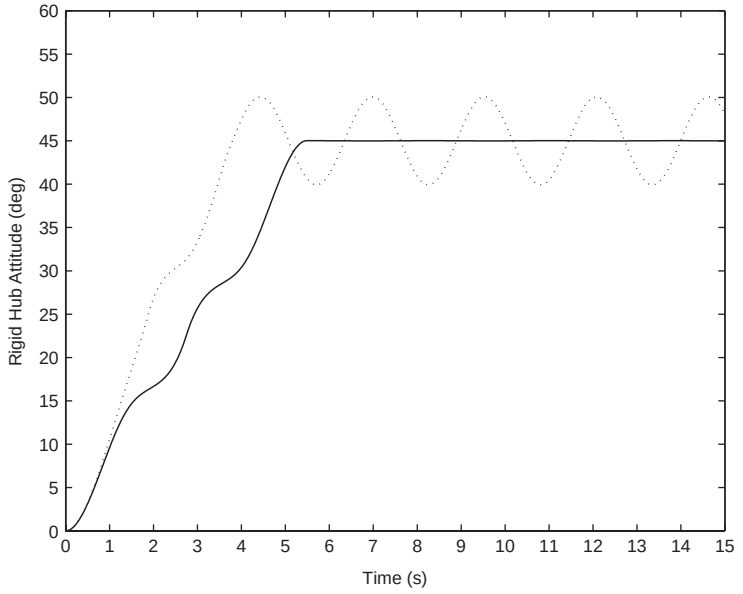

Fig. 12. Rigid hub attitude simulations without control mass (dotted, $t_f = 3.7719$ s, residual energy = 9.4356 J) and with control mass (solid, $m_c = 1.7$ kg, $x_c = 11.2$ m, $t_f = 5.4887$ s, residual energy = 0.00047 J) for the linear model.

amplitude has been reduced by 94%. As in Example 1, the slight disagreement between the linear and non-linear system model behaviors is attributed to the large tip mass deflection that is larger than $0.1L$, which is the maximum tip mass deflection allowed to neglect the non-linear terms in Eq. (13).

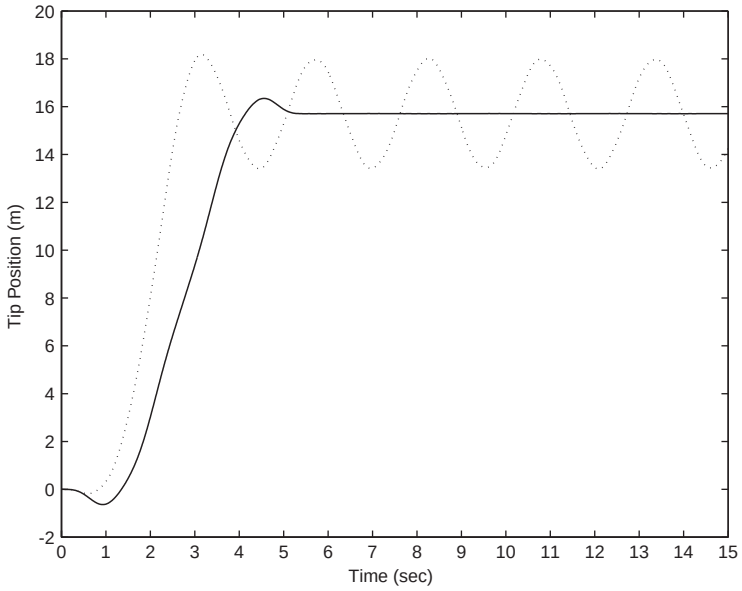

Fig. 13. Tip mass position simulations without control mass (dotted) and with control mass (solid, $m_c = 1.7$ kg and $x_c = 11.2$ m) for the linear model.

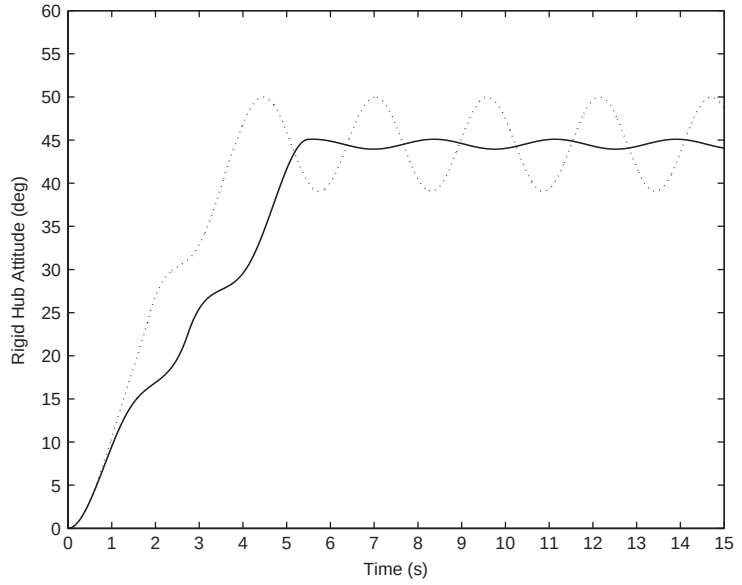

Fig. 14. Rigid hub attitude simulations without control mass (dotted, $t_f = 3.7719$ s, residual energy $= 11.0163$ J) and with control mass (solid, $m_c = 1.7$ kg, $x_c = 11.2$ m, $t_f = 5.4887$ s, residual energy $= 0.0718$ J) for the non-linear model.

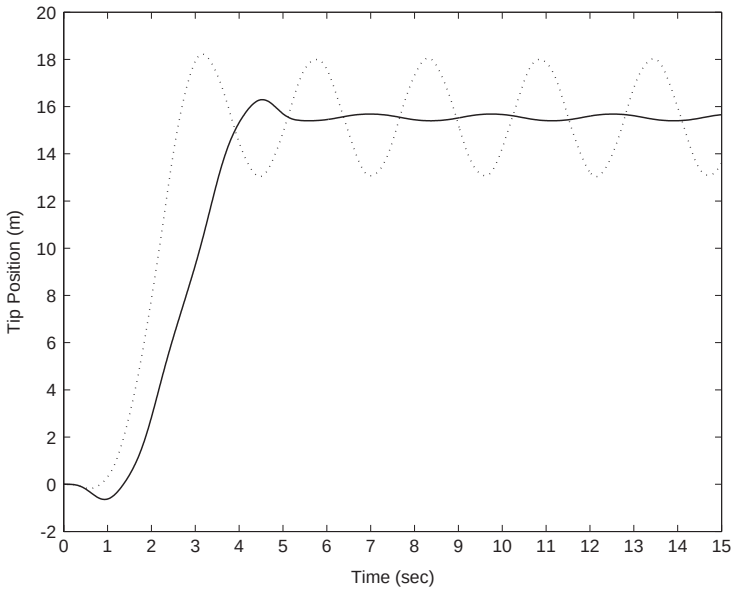

Fig. 15. Tip mass position simulations without control mass (dotted) and with control mass (solid, $m_c = 1.7$ kg and $x_c = 11.2$ m) for the non-linear model.

5. Experimental analysis

5.1. Experimental set-up

The experimental set-up is shown in Fig. 16. The flexible link is a slender beam made of stainless steel. The physical parameters of the experimental set-up and the associated sensors and actuators specifications are listed in Table 5. One end of the flexible link is clamped to a solid clamping fixture, which is driven by a high quality DC servomotor. The DC servomotor drives a built-in gearbox ($N = 14 : 1$) whose output drives an anti-backlash gear. The anti-backlash gear, which is equipped with a precision optical encoder to measure the flexible link base angle, is utilized to eliminate the backlash. The anti-backlash gear is connected to a larger gear with gear ratio 5 : 1 so that the angular displacement of the flexible link is further reduced. The tip deflection is measured using a strain gage mounted at the clamped end of the flexible link and is calibrated to generate one volt per one inch of tip deflection.

The DC servomotor is modelled as a standard armature circuit and the generated torque $u(t)$ can be related to the input voltage $V_a(t)$ as [19]

$$u(t) = N\frac{K_m}{R_a}V_a(t) - N^2 I_h\ddot{\theta} - N^2\left(\frac{K_m K_b}{R_a} + c_v\right)\dot{\theta}, \tag{26}$$

where N is the total gear ratio and is equal to $14 \times 5 : 1$, K_m is the motor torque constant, R_a is the armature resistance, I_h is the base inertia, K_b is the motor back emf constant and c_v is the viscous

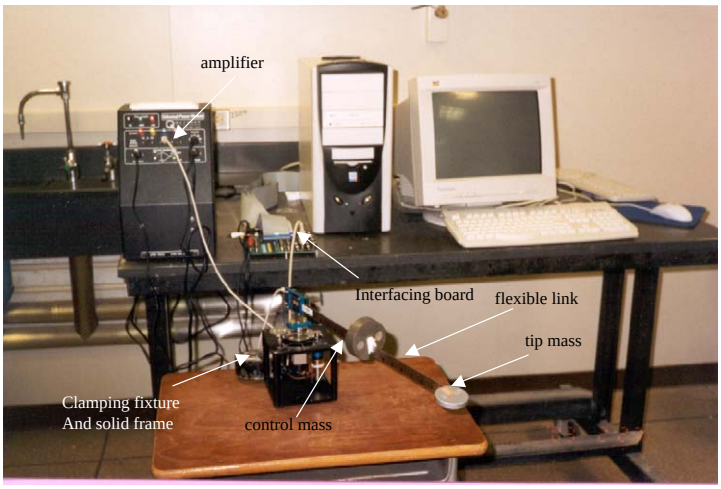

Fig. 16. Experimental set-up.

Table 5
Physical parameters for the experimental set-up

Flexible link		DC servo motor		Optical encoder	
Young's modulus	$E = 207 \times 10^9$ N/m^2	Motor back EMF constant	$K_b = 0.00767$ V/rad/s	Encoder resolution	4096 counts per revolution
Thickness	$b = 82$ mm				
Height	$h = 20.72$ mm	Motor torque constant	$K_m = 0.00767$ N m/amp		
Length	$L = 0.4318$ m				
Mass per unit length	$\rho = 0.135$ kg/m	Armature resistance	$R_a = 2.6\ \Omega$		
Base inertia	$I_h = 0.002$ kg m^2				
Tip mass	$m_t = 0.1$ kg	Equivalent viscous damping coefficient	$B_{\text{eq}} = 0.004$ N m/(rad/s)		
Tip inertia	$I_t = 0.0003$ kg m^2				
Gearbox ratio	$N = 70 : 1$				

damping in the motor. Eq. (26) can be substituted into Eq. (15) and the resulting uncoupled equations of motion for a one rigid-body mode and one flexible mode can be given as

$$\ddot{\beta} + b_0\dot{\beta} = a_0 V_a,$$
$$\ddot{\eta} + b_{11}\dot{\eta} + b_{12}\eta = a_1 V_a. \tag{27}$$

It is worth mentioning that the damping terms in Eqs. (27) are a result of the viscous damping in the motor. The time-optimal, bang–bang control input voltage applied to the motor, considering

only the rigid-body mode, the first equation in Eqs. (27), can be defined by calculating its switching and final times which are given by [17]

$$t_{s1} = \frac{1}{b_0}\ln\left(1 + \sqrt{1 - \exp\left(-\frac{b_0^2}{a_0 V_{a\,max}}\beta(t_f)\right)}\right) + \frac{b_0}{a_0 V_{a\,max}}\beta(t_f),$$

$$t_f = \frac{2}{b_0}\ln\left(1 + \sqrt{1 - \exp\left(-\frac{b_0^2}{a_0 V_{a\,max}}\beta(t_f)\right)}\right) + \frac{b_0}{a_0 V_{a\,max}}\beta(t_f), \tag{28}$$

where $V_{a\,max}$ denotes the magnitude of the applied voltage to the motor and $\beta(t_f)$ can be calculated using Eq. (22).

5.2. Experimental results

In this experiment, the flexible link base angular displacement and the tip deflection are to be measured, while the input signal is the applied voltage to the DC servomotor. The inputs and outputs from the experimental set-up are controlled through an 800 MHz, Pentium 4 PC computer. The computer is equipped with a data acquisition and control board (DACB) that contains 16 A/D channels, 8 D/A channels and 6 channels for digital encoder signals. The control voltage to the motor is applied through a digital signal processor (DSP) with sampling rate of

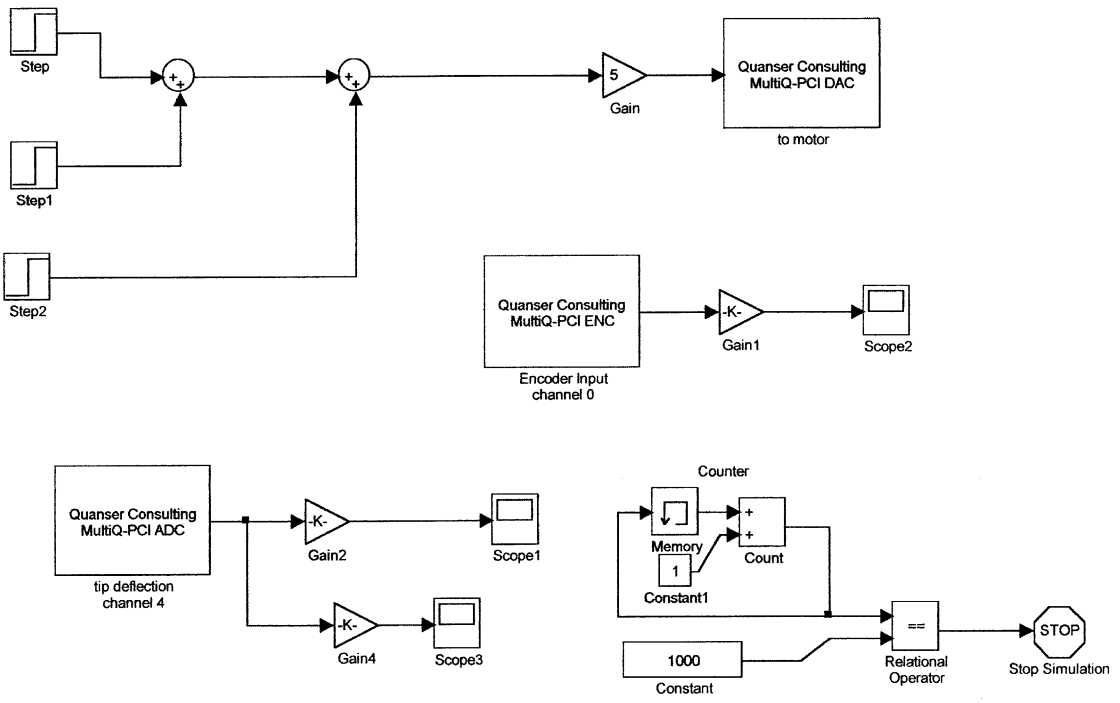

Fig. 17. Control algorithm implementation using Simulink®.

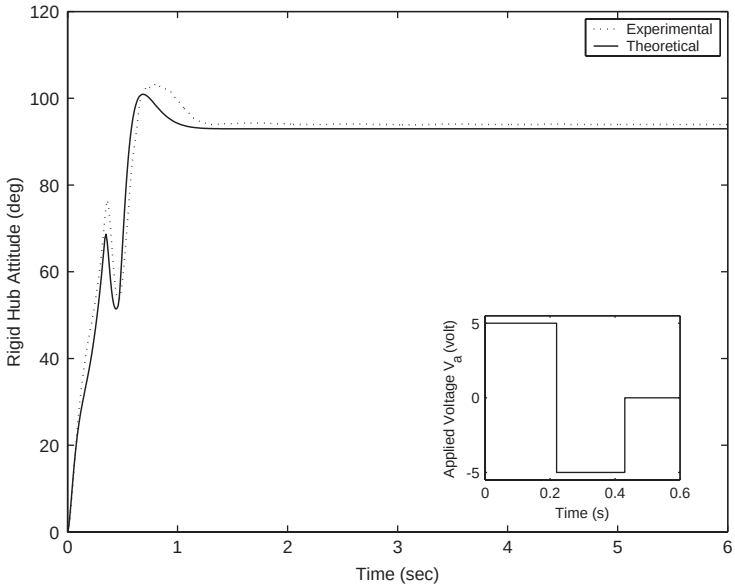

Fig. 18. Experimental and numerical results for the rigid hub attitude.

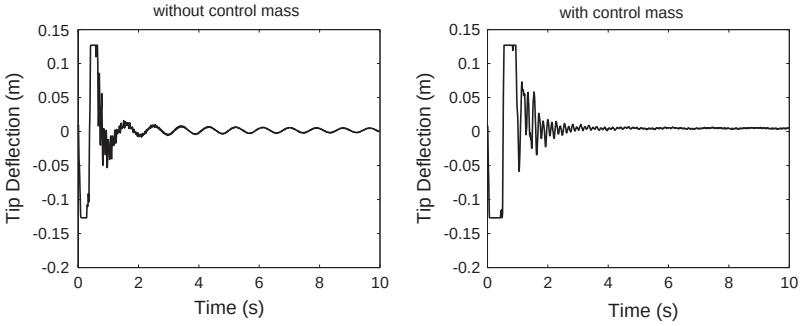

Fig. 19. Tip deflection obtained experimentally for the two cases: without and with control mass.

100 Hz. The data are also recorded at the rate of 100 Hz. The control algorithm is written in Simulink® and is shown in Fig. 17.

The mass and stiffness matrices, for the linear model in Eq. (15), are calculated as described in Section 2 using only one rigid-body mode and one flexible mode. The numerical and experimental rigid hub responses for a maximum applied voltage of 5 V and a maneuver of 90° are shown in Fig. 18. The close agreement between the two responses indicates an accurate mathematical model, and hence, a reliable calculation of the position and magnitude of the control mass can be obtained. A Matlab® program is developed that calculates the control mass position and magnitude that results in the minimum residual energy. The magnitude of the control mass, due to weight limitations of the experimental set-up, is limited to 0.5 kg. Therefore, the control mass magnitude is 0.5 kg while the calculated position is 0.264 m measured from the clamped end of the flexible link. The resulted residual energy has been reduced by 56% from 0.6801 to 0.2991 J for the

two cases without and with control mass, respectively. Consequently, the maneuver time has increased by 54% from 0.4675 to 0.7204 s for the two cases without and with control mass, respectively. The tip deflection for the cases without and with control mass, obtained experimentally, is shown in Fig. 19. As seen from this figure, the addition of the control mass has completely eliminated the vibration of the flexible link at the tip.

6. Conclusions

In this paper, a non-linear differential equations model is derived for a flexible structure comprising of a rigid hub with two elastic appendages, a tip mass and a control mass. The model is then linearized for controller design and implementation purposes. The control mass is a concentrated mass added to the system with the purpose of modifying the dynamic characteristics of the whole structure so that the application of the bang–bang control input for the rigid-body mode results in a negligible post-maneuver energy. In this way, the minimum-time property and simplicity of the bang–bang control input of the rigid-body mode are utilized while reducing the control spillover to the neglected flexible modes. A Matlab® program is written to assist in the selection of the control mass magnitude and position that results in negligible post-maneuver energy. To show the effectiveness of the design technique, the procedure is applied to both small and large size flexible structures, in which the control design method is able to eliminate the residual energy due to control spillover to the flexible modes at the expense of slight increase in maneuver time due to the addition of the concentrated mass. Experimental set-up has been developed to validate the derived mathematical model. The elimination of vibrations at the tip of the flexible link shown by experimental results proves the effectiveness of the control design method.

References

[1] T. Singh, S. Vadali, Robust time-optimal control: frequency domain approach, *Journal of Guidance, Control, and Dynamics* 17 (1994) 346–353.
[2] G. Singh, P. Kabamba, N. McClamroch, Planar, time-optimal, rest-to-rest slewing maneuvers of flexible spacecraft, *Journal of Guidance, Control, and Dynamics* 12 (1989) 71–81.
[3] Q. Liu, B. Wie, Robust time-optimal control of uncertain flexible spacecraft, *Journal of Guidance, Control, and Dynamics* 15 (1992) 597–604.
[4] J. Ben-Asher, J. Burns, E. Cliff, Time-optimal slewing of flexible spacecraft, *Journal of Guidance, Control, and Dynamics* 15 (1992) 360–367.
[5] S. Scrivener, R. Thompson, Survey of time-optimal attitude maneuvers, *Journal of Guidance, Control, and Dynamics* 17 (1994) 225–233.
[6] J.L. Junkins, Z. Rahman, H. Bang, Near-minimum-time control of distributed parameter systems: analytical and experimental results, *Journal of Guidance, Control, and Dynamics* 14 (1991) 406–415.
[7] N. Hecht, J.L. Junkins, Near-minimum-time control of a flexible manipulator, *Journal of Guidance, Control, and Dynamics* 15 (1992) 477–481.
[8] J. Hurtado, J.L. Junkins, Optimal near-minimum-time control, *Journal of Guidance, Control, and Dynamics* 21 (1998) 172–174.
[9] B.A. Albassam, Optimal near-minimum-time control design for flexible structures, *Journal of Guidance, Control, and Dynamics* 25 (2002) 618–625.

[10] R.F. Keltie, C.C. Cheng, Vibration reduction of a mass-loaded beam, *Journal of Sound and Vibration* 187 (1995) 213–228.
[11] Y. Chen, On the vibration of beams and rods carrying concentrated masses, *Journal of Applied Mechanics* 30 (1963) 310–311.
[12] L. Parnell, M. Cobble, Lateral displacement of a vibrating cantilever beam with a concentrated mass, *Journal of Sound and Vibration* 44 (1997) 499–511.
[13] J.L. Junkins, Y. Kim, *Introduction to Dynamics and Control of Flexible Structures*, AIAA, Washington, DC, 1993.
[14] W.J. Book, Modeling, design and control of flexible manipulator arms: a tutorial review, *Proceedings of the 29th IEEE Conference on Decision and Control*, Honolulu, Hawaii, 1990, pp. 500–506.
[15] M. Gu, S.F. Asokanthan, Combined discrete-distributed control of a single-link flexible manipulator using a Lyapunov approach, *Journal of Dynamic Systems, Measurement and Control* 121 (1999) 448–456.
[16] R.H. Cannon, E. Schmitz, Initial experiments on the end-point control of a flexible one-link robot, *The International Journal of Robotics Research* 3 (1984) 62–75.
[17] E. Ryan, *Optimal Relay and Saturating Control System Synthesis*, Peter Peregrinus, London, 1982.
[18] E. Barbieri, Single-input/single-output transfer functions for a flexible slewing link, *Journal of Robotic Systems* 10 (1993) 913–929.
[19] E. Garcia, D.J. Inman, Modeling of the slewing control of a flexible structure, *Journal of Guidance, Control, and Dynamics* 14 (1991) 736–742.